Hsp70 is phosphorylated in a conserved response to DNA damage and contributes to cell cycle control

Thomas Moss[1,2], Alexandra Wooldredge[1,2], Koustav Bhakta[1,2], Matthew Cronin[1,2], Jason E. Gestwicki[3], Shaeri Mukherjee[1,2,4#]

[1]G.W. Hooper foundation, University of California at San Francisco, San Francisco, USA.

[2]Department of Microbiology and Immunology, University of California at San Francisco, San Francisco, USA.

[3]Department of Pharmaceutical Chemistry and the Institute for Neurodegenerative Diseases, University of California San Francisco, San Francisco, CA, USA

[4]Biohub, San Francisco, CA 94158

[#] - Corresponding author: shaeri.mukherjee@ucsf.edu

ABSTRACT

Hsp70s are essential molecular chaperones that are increasingly recognized to be regulated by post-translational modifications. Here, we show that phosphorylation of a conserved threonine (T495), previously shown to be exploited by a *Legionella pneumophila* kinase to inhibit Hsp70, occurs endogenously in human cells in response to DNA damage, particularly when base excision repair is overburdened. This modification is cell cycle dependent, and in yeast, phosphomimetic or phosphonull Hsp70 variants disrupt G1/S progression under normal and DNA-damaging conditions. Biochemically, the phosphomimetic T495E mutation locks Hsp70 in an open-like conformation without blocking substrate engagement. Together, our results reveal a conserved mechanism by which dynamic Hsp70 phosphorylation regulates the G1/S transition, and delays cell cycle progression during DNA damage, highlighting how pathogen-derived insights can uncover fundamental cell biology principles.

INTRODUCTION

Hsp70s are highly conserved molecular chaperones with wide-ranging roles in cellular homeostasis. At the core of their function is an ATP-driven conformational cycle: Hsp70s alternate between an open ATP-bound state and a closed ADP-bound state, enabling them to bind and release client proteins in a nucleotide-dependent manner[1]. Through this mechanism, Hsp70s participate in diverse biological processes, including protein homeostasis[1], metabolic regulation[2], the DNA damage response[3], and cell cycle control[4–6]. Beyond their central roles in cell biology Hsp70s have been implicated in the pathology of numerous diseases. For example, Hsp70s can inhibit amyloid-beta aggregation *in vitro* and reduce its accumulation in mouse neurons, suggesting protective roles in neurodegenerative diseases such as Alzheimer's disease[7,8]. Hsp70s are also overexpressed in various cancers and influence tumor cell survival and proliferation [9]. Thus, understanding how Hsp70 activity is regulated has broad implications for both basic biology and therapeutic development.

Hsp70 function is tightly controlled by co-chaperones and post-translational modifications (PTMs). Cochaperones — namely J proteins and nucleotide exchange factors — catalyze nucleotide hydrolysis and exchange, facilitate and specify client engagement, and determine client fate [1]. In recent years, PTMs have emerged as an important layer of regulation. A computational analysis of the budding yeast Hsp70, Ssa1, identified two conserved 'hotspots' in the nucleotide binding domain (NBD) and substrate binding domain (SBD), that are likely regions of PTM-mediated regulation[10]. Experimental work has validated some of the PTMs at these site. For example, T36 in the NBD of Ssa1 is phosphorylated both in response to nutrient stress and exposure to mating pheromone (α-factor), impairing chaperone activity and leading to cell cycle arrest[4]. In mammalian cells, the endoplasmic reticulum (ER) resident Hsp70, BiP, is AMPylated at T518, locking it in an 'open' conformation and tuning its activity to the unfolded protein burden in the ER[11,12]. Our lab previously showed that the *Legionella pnuemophila* (*L.p.*) kinase LegK4 phosphorylates cytosolic human Hsp70 (Hsc70; HSPA8) at T495 during infection, increasing its association with polysomes and globally reducing protein synthesis[13]. Notably, Hsc70(T495) is structurally analogous to BiP(T518), indicating that both AMPylation and phosphorylation at this site have regulatory consequences. This finding led us to ask whether phosphorylation at T495 occurs outside of *L.p.* infection, and if it serves endogenous regulatory functions. Mining phosphoproteomics datasets revealed that the homologous residue in *S. cerevisiae* Ssa1, T492, is phosphorylated during DNA alkylation damage, and when mitotic exit is prevented[14,15]. However, the functional consequences of this modification have not been studied. In this work, we show that Hsp70 is phosphorylated at T495 (pHsp70) in human cells during base excision repair (BER) of DNA damage. We find that a phosphomimetic mutant T495E allosterically impairs ATP hydrolysis *in vitro* and stabilizes an open-like conformation while still permitting substrate engagement. In yeast, the analogous mutation T492E causes a growth defect, leads to accumulation of cells in G1, and delays cell

cycle re-entry after alkylation damage. Likewise, the phosphonull mutation (T492A) in yeast lacking a compensatory Hsp70 homolog also causes a growth defect and cell cycle dysregulation after alkylation damage. Together, these data suggest that the dynamic phosphorylation of Hsp70 at this conserved site acts as a regulatory switch to tune chaperone activity in coordination with DNA repair and cell cycle progression.

RESULTS

Phosphomimetic Hsc70 (T495E) is locked in an open-like conformation

Previous work showed that the *Legionella pneumophila* kinase LegK4 phosphorylates Hsc70 at a conserved threonine (T495) in its substrate binding domain (SBD) (Figure 1a,b)[13]. Investigations into the ATPase activity and refolding capacity of *in* vitro phosphorylated Hsc70 indicated that phosphorylation at T495 reduces its chaperone activity[13]. However, *in vitro* phosphorylation by LegK4 only yields phosphorylation of ~53% of the Hsc70, complicating bulk biochemical analyses[13]. To overcome this limitation, we generated a phosphomimetic mutant Hsc70 (T495E). To determine whether this mutant mimics phosphorylated Hsc70, we assessed the ATPase activity of the purified protein using a malachite green assay. As Hsc70 has a low intrinsic rate of ATPase activity, we titrated in the co-chaperone DnaJA2 to stimulate hydrolysis[13,16]. T495E exhibited significantly reduced J-protein stimulated ATPase activity compared to wild-type Hsc70 (WT) (Figure 1c), consistent with prior observations of the LegK4-phosphorylated protein[13]. To investigate if the reduced ATPase activity is due to impaired nucleotide binding, we performed a fluorescence polarization (FP) assay using fluorescently-labeled ATP-FAM. ATP binding was not diminished in T495E (Figure 1d), suggesting that T495E allosterically inhibits J protein stimulated ATPase activity without preventing nucleotide binding.

Hsp70 chaperone activity is driven by cycling through nucleotide-dependent conformations[1]. In the ATP-bound state, Hsp70s adopt an 'open' conformation, and ATP hydrolysis to ADP induces large-scale structural rearrangements to a 'closed' state[1]. As T495E poorly hydrolyzes ATP, we reasoned that this mutation may lock the protein into either the open or closed conformation. Indeed, AMPylation of BiP at the analogous residue is known to lock the protein in an open state[17]. To assess the conformation of T495E Hsc70, we performed partial proteolysis using trypsin, which produces distinct cleavage patterns depending on the protein's conformation[18,19]. As expected, WT Hsc70 displayed nucleotide-dependent banding: protection of band 2 and loss of band 3 in the presence of ADP compared to ATP. In contrast, T495E exhibited an ATP-like banding pattern regardless of nucleotide, consistent with a locked open conformation (Figure 1e). While this agrees with the studies on BiP AMPylation, our previous work showed that phosphorylation coincides with increased occupancy of Hsc70 on polysomes, suggesting continued substrate engagement[13]. We therefore asked whether T495E can still bind client proteins. An ELISA with tau, a known Hsc70 substrate[20], showed that T495E retains the ability to bind tau despite the conformational lock (Figure 1f). These results suggest that T495E locks Hsc70 in a pseudo-open conformation: structurally similar to the ATP-bound open state in terms of protease sensitivity and domain exposure, yet still capable of substrate engagement typically associated with the closed state.

Base excision repair leads to Hsp70(T495) phosphorylation

Pathogens often mimic host proteins and hijack cellular pathways to create a favorable niche for replication. Thus, these pathogen-driven modifications frequently reveal biologically significant regulatory nodes within host systems[21]. Given this tendency of pathogens and the high degree of conservation of T495 (Figure 1b), we reasoned that *L.p.* phosphorylation of Hsp70 may be targeting an important regulatory module. Motivated by this concept, we examined published phospho-proteomics datasets to determine if this phosphorylation had been previously observed

151 in eukaryotes. A phospho-proteomics study in *S. cerevisiae* identified phosphorylation at the
152 analogous residue, Ssa1(T492), after treatment with the alkylating agent methyl
153 methanesulfonate (MMS)[14]. Inspired by this finding, we analyzed human cells treated with MMS
154 and observed that this phosphorylation is conserved(Figure 2a). As expected, this band is
155 sensitive to phosphatase activity (Figure S1a).
156 This finding suggested that phosphorylation of Hsp70 might be involved in the response
157 to DNA damage. MMS is primarily used as a DNA alkylating agent, though its chemical activity is
158 not limited to DNA targets[22]. Thus, we sought to determine whether the response to MMS-induced
159 DNA alkylation leads to Hsp70 phosphorylation. Aberrant DNA alkylation is predominantly
160 repaired through the base excision repair (BER) pathway[23]. In BER, DNA glycosylases recognize
161 and excise damaged bases, producing an abasic site (AP site). MMS-induced lesions are
162 processed by N-methylpurine DNA glycosylase (MPG)[23,24] (Figure 2b). The backbone at the AP
163 site is then cleaved by the endonuclease APE1, and the resultant single stranded break is
164 repaired by a variety of proteins, including the DNA polymerase Polβ[23] (Figure 2b). Interestingly,
165 the predominant DNA adduct generated by MMS, 7-methylguanine, is not intrinsically cytotoxic,
166 but spontaneously depurinates to a toxic and mutagenic intermediate and so requires rapid
167 repair[25,26]. The repair intermediates generated by the BER pathway, however, are cytotoxic[25,27].
168 Because Polβ activity is rate limiting, overexpression of the glycosylase that initiates BER can
169 lead to an accumulation of these cytotoxic intermediates[23,28]. To determine whether increased
170 BER activity affects Hsp70 phosphorylation, we treated cells overexpressing MPG with MMS.
171 MPG overexpression modestly increased MMS-induced pHsp70 levels (Figure 2c). Conversely,
172 inhibition of the subsequent BER step strongly reduced the levels of MMS-induced pHsp70.
173 Pharmacological inhibition of APE1 led to a dose dependent decrease in Hsp70 phosphorylation
174 (Figure 2d). Similarly, treatment with methoxyamine (Mx), which covalently binds AP sites and
175 impairs APE1 cleavage and Polβ activity[29], caused a striking reduction in pHsp70 levels (Figure
176 2b,e). Surprisingly, overexpression of APE1 did not enhance pHsp70 (Figure S1b), suggesting
177 that APE1 activity is necessary but not rate-limiting in this context. Additionally, overexpression
178 of Polβ did not reduce pHsp70 upon MMS treatment (Figure S1c). These data confirm that the
179 DNA alkylation by MMS is responsible for Hsp70 phosphorylation in human cells, and the results
180 specifically indicate that BER intermediates may trigger this response.
181 To test the specificity of Hsp70 phosphorylation in response to DNA damage, we treated
182 cells with a panel of genotoxic compounds that activate distinct branches of the DNA damage
183 response (DDR), including bleomycin (induces double stranded breaks), camptothecin (a
184 topoisomerase I inhibitor), hydroxyurea (depletes the dNTP pool), MMS, and arsenite (generates
185 reactive oxygen species). While activation of DDR kinases (pDNA-PKcs(S2056), pATM(S1981)
186 pChk2(T68), pChk2(S516)), and an increase of the DDR marker γH2AX confirm DNA damage
187 and response induction in the drug treatment conditions, pHsp70 was only observed following
188 high-dose MMS treatment, and exposure to sodium arsenite (Figure 2f). Arsenite causes
189 oxidative DNA damage that can be repaired through BER[23,30]. Surprisingly, arsenite has also been
190 shown to both inhibit the activity of enzymes necessary for this pathway, including OGG (the
191 oxidative glycosylase)[31], and decrease the levels of others (e.g. APE1 and Polβ) [32]. Despite this,
192 we found that both treatment with Mx and inhibition of APE1 were still sufficient to prevent Hsp70
193 phosphorylation upon arsenite treatment (Figure S1d,e). These findings suggest that Hsp70(T495)
194 phosphorylation is selectively triggered by repair intermediates generated during BER.
195
196 **Phosphorylation of Hsp70 requires the DDR kinases ATM, DNA-PKcs, Chk2, and CK1**
197 Ape1 activity generates cytotoxic adducts. Its endonuclease activity at abasic sites directly
198 generates single stranded DNA breaks (SSBs)[33]. These SSBs can in turn convert to DSBs
199 through two primary mechanisms: collision of a replication fork with the SSB[33–35]; or generation of
200 SSBs in proximity on opposing strands of DNA[36]. In these cases, damaged DNA is sensed and a

response subsequently mounted through DDR pathways. At the highest level, the varied branches of the DDR are controlled by three master kinases: ataxia-telangiectasia mutated (ATM), ataxia-telangiectasia and Rad3-related (ATR), and DNA-dependent protein kinase (DNA-PK). ATR orchestrates the response to SSBs, while ATM and DNA-PK direct DSB repair through homologous recombination (HR) and non-homologous end joining (NHEJ), respectively[37,38]. While this broadly describes the organization of the DDR, the apparent simplicity belies the fact that these master regulators induce varied and nuanced responses depending on the exact type and severity of DNA damage present[39–42].

To determine if DDR signaling contributes to MMS-induced Hsp70 phosphorylation, we performed siRNA-mediated knockdowns of these three master kinases. Among these, only knockdown of DNA-PKcs prevented Hsp70 phosphorylation (Figure 3a, Supp Figure 2a,b). Interestingly, while ATM knockdown had no effect, pharmacological inhibition of ATM decreased Hsp70 phosphorylation (Figure 3b). To rule out off-target effects, we tested two independent ATM inhibitors and observed a similar reduction in pHsp70 with both (Figure 3b). This discrepancy is consistent with prior reports showing that genetic and pharmacological inhibition of ATM can yield diverging results[43,44]. Pharmacological inhibition of DNA-PKcs confirmed the DNA-PKcs knockdown experiment (Figure 3c). Both DNA-PKcs and ATM phosphorylate the transducer kinase Chk2, activating it and promoting propagation of the DDR[45]. Inhibition of Chk2 also prevented Hsp70 phosphorylation (Figure 3c). Given that casein kinase 1 (CK1) has been previously reported to act in concert with Chk2 in the DDR[46], we tested its involvement and found that CK1 inhibition also suppressed Hsp70 phosphorylation (Figure 3d, Figure S2c). Inhibition of these kinases also prevented Hsp70 phosphorylation upon arsenite treatment (Figure S2d).

While these kinases appear to be necessary for Hsp70 phosphorylation, our data are more consistent with their involvement in upstream signaling rather than directly acting on Hsp70. We would further highlight that the delay in Hsp70 phosphorylation contrasts with canonical DDR signaling, which is initiated within minutes of damage induction,[47,48] pHsp70 only emerges after prolonged MMS exposure (Fig 3d). Indeed, we observed robust activation of DNA-PKcs, ATM and Chk2 well before Hsp70 phosphorylation (Figure 3d). These observations raise the possibility that either prolonged MMS exposure or a secondary cellular response is required to trigger Hsp70 phosphorylation.

Hsp70 phosphorylation occurs after M phase onset

To better understand the timing of Hsp70 phosphorylation, we treated cells with MMS for varying durations (1 to 5 hours), followed by recovery in fresh media up to a total of 5 hours. In previous experiments, we observed robust Hsp70 phosphorylation only after 5 hours of continuous MMS treatment, with minimal signal at earlier timepoints (see Fig. 3d). However, in our pulse-chase assay, 2 hour MMS treatment, when followed by a 3 hour MMS-free chase, resulted in pHsp70 accumulation (Fig. 4a). This result indicates that prolonged MMS exposure alone does not fully explain the lag time between damage initiation and the appearance of pHsp70, suggesting that secondary cellular events or signaling contribute to Hsp70 phosphorylation.

Damage from MMS is thought to occur when replication forks collide with DNA repair intermediates in S phase[34,35]. This hypothesis, in combination with our observations that pHsp70 accumulation lags behind initial DDR activation, suggested that cell cycle stage might be a key determinant in Hsp70 phosphorylation. In asynchronous populations, Hsp70 phosphorylation might only appear when enough cells reach a permissive phase of the cell cycle. If this were true, synchronizing cells at the beginning of S phase should potentiate MMS-induced Hsp70 phosphorylation. To test this idea, we synchronized cells at the beginning of S phase using a double thymidine block, then released them into MMS-containing or untreated media. Unexpectedly, synchronization at G1/S does not increase Hsp70 phosphorylation (Figure 4b). Even more surprising, MMS-treated cells entered mitosis at an increased rate compared to controls, as evidenced by the accumulation of the mitotic marker phospho-Histone H3 (S10) (pH3),

252 reduced levels of S phase markers such as the replication licensing factor CDT1 and thymidine
253 kinase, and pCdk1 (Y15), the inhibited cyclin dependent kinase that must be de-phosphorylated
254 for M phase entry (Figure 4b). These data suggest that MMS drives cells into mitosis, and that
255 Hsp70 phosphorylation occurs after this transition. Indeed, blocking mitotic entry by treatment
256 with a CDK1 inhibitor (Ro3306) prevented both MMS and arsenite induced Hsp70
257 phosphorylation (Figure 4c, Figure S3a). Releasing the CDK1 block upon MMS or arsenite
258 treatment restored Hsp70 phosphorylation (Figure 4c, Figure S3a), suggesting this response does
259 not require passage through S phase. While passage through mitosis upon DNA damage is
260 necessary for Hsp70 phosphorylation, the presence of pHsp70 in a distinct nuclear fraction
261 indicates that it persists after nuclear envelope reformation (Figure 4d). Indeed, a 2 hour pulse
262 chase of MMS revealed that pHsp70 accumulates even after pH3 disappears, indicating that
263 phosphorylation is maintained after mitotic exit (Figure 4e). Notably, we do not see an increase
264 of S phase markers such as thymidine kinase, nor changes in cyclin A or cyclin B levels,
265 suggesting that the cell cycle progression may be dysregulated following MMS treatment.
266
267 **Phosphoregulation of Ssa1 at T492 is important for G1/S transition in yeast**
268 To investigate the functional significance of Hsp70 phosphorylation at T495, we turned to
269 *S. cerevisiae* due to its genetic tractability. *S. cerevisiae* has four cytosolic Hsp70s, Ssa1-4. Of
270 these, Ssa1 and Ssa2 are constitutively expressed, whereas Ssa3 and Ssa4 are stress-
271 inducible[49]. Phosphoproteomics studies revealed that Ssa1 can be phosphorylated at threonine
272 492, which corresponds to human Hsp70 T495[14,15]. To probe the role of this modification, we
273 created phosphomimetic (T492E, TE) and phosphonull (T492A, TA) point mutations at the
274 endogenous *SSA1* locus. Given the known redundancy between Ssa1 and Ssa2[50], we disrupted
275 *SSA2* by inserting an antimicrobial resistance gene into its coding sequence to better assess the
276 functional consequences of Ssa1 phospho-variants. To confirm the conservation of Hsp70
277 phosphorylation in yeast, we treated our mutants with MMS as previously described[14] and
278 performed a Western blot. Notably, we see faint pHsp70 signal in WT yeast in the absence of
279 MMS treatment (Figure 5a). This corresponds with prior work indicating low levels of phospho-
280 Ssa1 (T492) in asynchronously growing cells.[15] This signal is diminished in the phosphomutant
281 strains, and in all *ssa2*Δ strains, both supporting the conclusion that our antibody binds
282 pHsp70(T492) in yeast, and indicating that there is likely redundant phospho-regulation of Ssa2
283 as well. Additionally, we find that MMS treatment leads to a strong increase in Hsp70
284 phosphorylation in WT, and phosphorylation to a lesser extent in WT;*ssa2*Δ (Figure 5a). Strikingly,
285 even in the *SSA2* background, we observed a growth defect in TE yeast (Figure 5b,c). This is not
286 likely explained by hypomorphism, as neither the TA mutant nor the WT;*ssa2*Δ strains show such
287 a defect. Rather, phosphomimetic Ssa1 seems to act in a dominant-like manner. In the *ssa2*Δ
288 background, strains expressing either phosphomimetic or phosphonull Ssa1 grew more slowly
289 than the wild-type (Figure 5 b,c).
290 Phosphorylation of Ssa1 at T492 was previously reported to occur in a cell cycle
291 dependent manner, specifically when yeast are prevented from exiting mitosis through the
292 expression of a non-degradable cyclin B[15]. This information, in conjunction with the cell cycle
293 dependence of pHsp70 in human cells and the growth defects we observed in our yeast
294 phosphomutants, led us to examine the impact of these mutations on cell cycle progression. With
295 SSA2 present, the Ssa1 WT and phosphonull (TA) strains showed similar cell cycle distributions.
296 In contrast, the phosphomimetic mutant (TE) showed an increase in cells with 1N DNA content,
297 consistent with a G1 stall (Figure 5d). In the *ssa2*Δ background for both Ssa1 WT and TA, we see
298 a slight increase in the G1 population compared to G2, and the difference is even more
299 pronounced in T492E yeast (Figure 5d). T492A yeast showed increased cell size in G1 in the
300 *ssa2*Δ background, a phenotype previously linked to G1/S stalling, perhaps due to decreased
301 Cln3 stability or disrupted Cln3-Ssa1 interactions[4,51] (Figure S3a). Intriguingly, both *ssa2*Δ point
302 mutants exhibited a large cell size in G2/M (Figure S3a) — a finding that warrants additional

303 investigation. Together, these data suggest that dynamic phospho-regulation of Ssa1 at T492 is
304 critical for proper cell cycle progression.
305 We were curious if this modification served a similar cell cycle regulatory function during
306 MMS treatment. To assess the overall viability of the point mutants in response to alkylation
307 damage we performed a spot test in the presence and absence of MMS. In the *ssa2*Δ background,
308 both phosphonull and phosphomimetic Ssa1 led to impaired growth on MMS-containing media,
309 though growth in the in the *SSA2* background was only mildly impacted (Figure 5e). To examine
310 how these mutations influence cell cycle progression in response to MMS, we treated the strains
311 with 0.05% MMS for three hours as previously shown to cause Ssa1 phosphorylation at T492[14],
312 and released them into fresh YPAD for the indicated times (Figure 5f). Ssa1 WT strains with and
313 without *SSA2* behave similarly: immediately after the MMS treatment the cells display a bimodal
314 distribution around G1 and early S. Upon MMS release, the G1 peak gradually disappeared,
315 accompanied by synchronized progression through S phase, with DNA content slowly increasing
316 over time. In the *SSA2* background, the T492A was nearly indistinguishable from the WT strains.
317 However, in the *ssa2*Δ background, T492A no longer exhibited the bimodal distribution of cells
318 near 1N immediately after MMS treatment. Rather, there was a single peak. Upon release, the
319 cells failed to undergo coordinated S phase progression. Instead, DNA content increased in an
320 asynchronous manner, suggesting impaired checkpoint regulation. The T492E mutants also
321 showed distinct phenotypes. In the *SSA2* background, T492E cells lacked the bimodal distribution
322 around 1N immediately after MMS treatment, and instead exhibited a more pronounced G1 arrest.
323 Upon release, these cells progressed through S phase more slowly than WT, with a prominent
324 left shoulder, indicating delayed DNA replication in a subset of cells. In the *ssa2Δ* background,
325 the phenotype was even more prominent. A strong 1N peak persisted after MMS release, with
326 minimal evidence of bulk S phase progression. Instead, we observed a gradual increase in DNA
327 content across the population, reminiscent of the T492A mutant in *ssa2Δ*, but with a key difference:
328 while T492A;*ssa2*Δ cells showed more rapid entry to and passage through S phase, T492E;*ssa2Δ*
329 cells retained a distinct 1N peak and slower S phase progression. These data indicate that both
330 phosphonull and phosphomimetic mutations disrupt the coordination of cell cycle re-entry
331 following genotoxic stress. Loss of phosphorylation appears to weaken G1 arrest and promote
332 uncontrolled S-phase entry, while constitutive phosphorylation reinforces arrest but impairs
333 orderly progression through S-phase. Eliminating the functional redundancy of Ssa2 in the
334 T492A;*ssa2*Δ and T492E;*ssa2*Δ strains reveals the importance of dynamic Ssa1 phospho-
335 regulation in mounting an effective DNA damage response and ensuring proper cell cycle
336 transitions**,** as both phosphonull and phosphomimetic Ssa1 variants result in cell cycle
337 dysregulation and altered growth in the absence of Ssa2.
338
339 **DISCUSSION**
340 Our work demonstrates that Hsp70s are phosphorylated at T495 as part of a conserved
341 response to DNA damage, and that dynamic phosphoregulation of this residue exerts control over
342 the cell cycle. While prior phosphoproteomics studies in yeast detected phosphorylation of the
343 analogous residue in Ssa1 (T492) following MMS exposure[14] or mitotic exit block[15], our findings
344 establish that this modification is a regulated, damage-responsive event that is conserved in
345 human cells. We show that phosphorylation is induced by two chemically distinct DNA-damaging
346 agents, MMS and sodium arsenite, both of which generate BER substrates. Critically, inhibition
347 of the BER endonuclease APE1 or chemical blockade of abasic site recognition and repair
348 abolishes pHsp70 formation. Of note, high doses and long treatment times are required to elicit
349 Hsp70 phosphorylation with both compounds, which raises questions as to the precise driver of
350 this response. One caveat to this lies in our bulk detection method: the use of whole-cell lysate
351 for Western blotting seems to dilute pHsp70 signal at earlier time-points, such that longer MMS
352 treatment is required for sufficient pHsp70 to accumulate. This is illustrated by the fact that
353 pHsp70 appears earlier in nuclear fractions that in whole-cell lysate (Figures 4d, 3d). While it is

354 important to keep this limitation in mind, the dose and timing of insult still merits consideration.
355 BER is a streamlined pathway: it is thought to follow a 'baton-passing' model, with each enzyme
356 passing off intermediates to the next in the cascade[52]. However, BER intermediates are cytotoxic.
357 APE1-mediated cleavage of the DNA backbone produces single-strand breaks that, if
358 encountered by replication forks, can be converted into double-stranded breaks (DSBs)[34,35]. The
359 requirement for APE1 activity, along with the involvement of the DSB repair kinases ATM and
360 DNA-PKcs, support a model in which BER-induced DSBs lead to Hsp70 phosphorylation. While
361 it is true that pharmacological inhibition and siRNA-mediated knockdowns can have off target and
362 pleiotropic effects[53,54], our use of orthogonal approaches to perturb the aforementioned pathways
363 in conjunction with knowledge that both MMS and sodium arsenite generate lesions repaired by
364 BER leads us to believe that the parsimonious explanation is that phosphorylation of Hsp70 is
365 downstream of a DNA damage response[23,24,30].
366 While it is clear that Hsp70 is phosphorylated in response to DNA damage, the lag time
367 between insult and pHsp70 suggests a complex signaling pathway. Phosphorylation does not
368 arise simply during damage exposure; instead, it requires both prolonged insult and progression
369 through mitosis. Despite the longstanding view that MMS-induced damage primarily arises during
370 S phase, we find that synchronizing cells at G1/S does not enhance Hsp70 phosphorylation. This
371 paradox may be resolved by emerging evidence that BER-induced DSBs can occur in non-
372 replicating cells[36]. Considering that the DDR is considerably rewired during mitosis, and though
373 BER occurs, repair of lesions such as DSBs is forestalled until mitotic exit[41,55,56], it is possible that
374 pHsp70 arises in response to high lesion burden in M phase to prevent cell cycle entry into the
375 vulnerable S phase.
376 Our genetic studies in yeast directly link phosphoregulation of Ssa1 at T492 to cell cycle
377 progression. Both phosphonull (T492A) and phosphomimetic (T492E) mutants cause growth
378 defects in the absence of the compensatory isoform Ssa2, underscoring the importance of
379 dynamic, reversible phosphorylation at this site. Alternatively, it is possible that the phosphonull
380 mutation is not neutral and thus exhibits additional affects. Future work should examine the
381 biochemical consequences of this mutation to clarify our findings. Cell cycle profiling reveals that
382 T492E yeast in both *SSA2* and *ssa2*Δ backgrounds accumulate in G1 and fail to efficiently enter
383 S phase following MMS exposure, while T492A strains show delayed recovery in the absence of
384 Ssa2. Further, in the absence of MMS insult, the Ssa1 T492E mutant strain exhibits altered growth
385 and cell cycle progression even in the *SSA2* background, suggesting a dominant-like effect of the
386 phosphomimetic variant. The dominant-like phenotype of T492E is consistent with biochemical
387 data suggesting persistent, aberrant substrate engagement, akin to the effects of mutations that
388 trap Hsp70 in a closed conformation[57]. Together, these results support a model in which pHsp70
389 serves as a reversible molecular brake, preventing premature S-phase entry under conditions of
390 BER stress.
391 Interestingly, this mechanism parallels, but is distinct from the previously described
392 phospho-Ssa1 (T36) mediated regulation of the cell cycle. Phosphorylation at T36/38 also
393 enforces G1/S arrest in yeast. However, the residue is in the NBD, and phosphorylation
394 decreases nucleotide binding. Furthermore, the activity is ER-localized, where it slows the
395 accumulation of Cdk1-Cln3 by sequestering and promoting the degradation of Cln3[4]. In contrast,
396 pT492/495 occurs in the SBD, modulates ATP hydrolysis without preventing nucleotide binding,
397 and occurs in the nucleus. Given the established role of phosphorylation in directing Hsp70-client
398 fate[58,59,67], it is plausible that pT492/T495 controls the stability or activity of nuclear substrates
399 critical for G1/S transition. Our data support a model wherein Hsp70 engagement with both a
400 client and some accessory machinery (e.g. a cochaperone) are controlled by phosphorylation to
401 regulate S phase entry. For instance, if a specific Hsp70 client must be degraded to exit G1,
402 phosphorylation may promote engagement with said client and proper degradation machinery,
403 and dephosphorylation could allow client release. In this case, the phosphomimetic Hsp70 would
404 be unable to disengage, and therefore cause the G1/S stall we report. Conversely, the

phosphonull Hsp70 would be unable to establish proper interactions with the client and/or accessory machinery, thereby preventing efficient degradation and leading to the observed dysregulation of S phase re-entry. While this model explains our experimental observations, other possibilities remain, and future work is required to further establish mechanistic details.

Collectively, our findings reveal a conserved phospho-switch on Hsp70 that links DNA damage sensing during BER to cell cycle control, adding an unanticipated regulatory layer to the integration of repair and checkpoint pathways. Strikingly, this pathway came to light because it is targeted by a pathogenic effector kinase, once again illustrating how pathogens can hijack, and thereby illuminate, fundamental aspects of cell biology. Such examples underscore the enduring value of pathogens as powerful tools to uncover deeply conserved regulatory mechanisms. This work opens the door to identifying the upstream kinase(s) and downstream client(s) that mediate this effect, and to determining whether T495 phosphorylation serves as a general mechanism for coordinating repair with proliferation in diverse physiological contexts. By coupling BER to a reversible molecular brake on S phase entry, phosphorylation of Hsp70 at T495 emerges as a conserved checkpoint signal that safeguards genome integrity under conditions of repair-induced stress.

During the revision of this manuscript, Omkar et al. reported heat shock–induced phosphorylation of this residue in *S. cerevisiae* via the Cell Wall Integrity (CWI) pathway,[66] consistent with the regulatory potential we describe here.

456 **KEY RESOURCES**

457 Plasmids

Description	ID	Source
Hsc70 in pMCSG7	pSM226	Moss 2019[13]
Hsc70(T495E) in pMCSG7	pSM227	Moss 2019[13]
LegK4Δ1-58 in pEGFP-C2	pSM160	Moss 2019[13]
MPG in pIRESNeo	pSM282	Addgene Plasmid #12548
APE1 in pCMVd3	pSM303	This study
pCMVd3 empty vector	pSM304	This study
Polβ in pLVX-GWE-IRES-puro	pSM288	Addgene Plasmid #128653
plVX-GWE-IRES-puro empty vector	pSM289	This study
pYM13 PCR template KanMX resistance	pSM302	Gift from David O. Morgan Lab

458

459 RNA Oligos

Description	Sequence
siDNA-PKcs #1	GCGUUGGAGUGCUACAACA[dT][dT]
siDNA-PKcs #2	CAAGCGACUUUAUAGCCUU[dT][dT]
siDNA-PKcs #3	GACCCUGUUGACAGUACUU[dT][dT]
siATM #1	GCUGUUACCUGUUUGAAAA[dT][dT]
siATM #2	CACCUGUUUGUUAGUUUAU[dT][dT]
siATM #3	CAGCUGUCAUCAUAUAAGA[dT][dT]
siATR #1	GAGCCGAUUUUUAAGUCAA[dT][dT]
siATR #2	GAUGAGUAUGCAAAAUUUA[dT][dT]
siATR #3	GCCGCUAAUCUUCUAACAU[dT][dT]

460

461 DNA Oligos

Description	Sequence
SSA1 gDNA T492E Forward	TCGATGTCGACTCTAACGGTATTTTGAATGTTTCCGCCGTCGAAAAGGGTGAAGGTAAGTCTAACAAG
SSA1 gDNA T492A Forward	TCGATGTCGACTCTAACGGTATTTTGAATGTTTCCGCCGTCGAAAAGGGTGCTGGTAAGTCTAACAAG
SSA1 gDNA Reverse	CAGATCATTAAAAGACATTTTCGTTATTATCAATTGCCGCACCAATTGGCGCATGCCGGTAGAGG
SSA2-KanMx Forward	TTGATTAATTCCAACAGATCAAGCAGATTTTATACAGAAATATTTATACAATGGGTAAGGAAAAGACTCA
KanMx-Ssa2 Reverse	GGAAAGCAAAAGTAAAACTTTTCGGATATTTTACAGGGCGATCGCTAAGCTTAGAAAAACTCATCGAGCA

462

463 Antibodies

Antigen	Dilution	Supplier (catalog #)
pHsp70	1:5000	Custom (Moss 2019)[13]
GAPDH	1:3000	Proteintech (60004-1-Ig)
γH2AX	1:1000	Millipore Sigma (05-636)
Hsp70	1:1000	Santa Cruz Biotechnology (sc-66048)
pDNA-PKcs (S2056)	1:1000	Abcam (ab18192)
pChk2 (T68)	1:1000	Cell Signaling Technology (2197T)
Hsp90	1:1000	Cell Signaling Technology (4874S)
pChk2 (S516)	1:1000	Cell Signaling Technology (2669T)
pATM (S1981)	1:1000	Cell Signaling Technology (4526S)
Tubulin	1:3000	Proteintech (66031-1-Ig)
Thymidine Kinase	1:1000	Cell Signaling Technology (28755S)
pCdk1 (Y15)	1:1000	Cell Signaling Technology (4539S)
Cyclin B	1:500	Santa Cruz Biotechnology (sc-245)
pHistone H3 (S10)	1:1000	Cell Signaling Technology (53348S)
Cyclin E	1:1000	Santa Cruz Biotechnology (sc-247)
CDT1	1:1000	Cell Signaling Technology (8064S)
Lamin B1	1:1000	Proteintech (12987-1-AP)
Cyclin A	1:1000	Santa Cruz Biotechnology (sc-271682)
Polβ	1:1000	Proteintech (18003-1-AP)
APE1	1:1000	Proteintech (10203-1-AP)
ATM	1:1000	Cell Signaling Technology (2873S)
ATR	1:1000	Cell Signaling Technology (2790S)

464

465 Yeast Strains

Description	ID
Parental W303α	Y017
Ssa1(WT)-NAT #1	Y019
Ssa1(WT)-NAT #2	Y034
Ssa1(T492A)-NAT #1	Y040
Ssa1(T492A)-NAT #2	Y041
Ssa1(T492E)-NAT #1	Y038
Ssa1(T492E)-NAT #2	Y039
Ssa1(WT)-NAT;*ssa2*Δ #1	Y023
Ssa1(WT)-NAT;*ssa2*Δ #2	Y037

Ssa1(T492A)-NAT;*ssa2*Δ #1	Y051
Ssa1(T492A)-NAT;*ssa2*Δ #2	Y046
Ssa1(T492E)-NAT;*ssa2*Δ #1	Y044
Ssa1(T492E)-NAT;*ssa2*Δ #2	Y057

Software (all code available upon request)

Software	Source	URL
Prism Version 10.4.2	Graphpad	https://www.graphpad.com/scientific-software/prism/
ImageLab 6.0.1	Biorad	https://www.bio-rad.com/en-us/product/image-lab-software?ID=KRE6P5E8Z
FlowJo™ 10.10.0	BD Life Sciences	https://flowjo.com/flowjo/download
UCSF Chimera X v1.3	Pettersen et al.[60]	https://www.rbvi.ucsf.edu/chimera

METHODS

Cell Culture

HEK293T and HeLa lines were obtained from ATCC. All cell lines were regularly tested for mycoplasma contamination. Cells were maintained in Dulbecco's modified Eagle's medium (DMEM, Gibco) supplemented with 10% fetal bovine serum (FBS, VWR) in a humidified incubator at 37°C, 5% CO_2. Cells were treated with 10 mM methyl methanesulfonate (MMS) (Fisher AC156890050) for 5 h unless otherwise indicated. Cells were treated with methoxyamine hydrochloride (Sigma Aldrich 226904), APE1 compound III (EMD Millipore 262017), bleomycin (sulfate) (Thomas Scientific C830H18), camptothecin (Selleck S1288), hydroxyurea (Sigma-Aldrich H8627), sodium arsenite (Fisher Scientific S88733), KU-60019 (MedChem Express HY-12061), AZD1390 (MedChem Express 2089288-03-7), CCT241533 (MedChem Express HY-14715B), PF-670462 (Sigma-Aldrich SML0795), thymidine (Fisher 501882638), Ro-3306 (MedChem Express HY-12529), and AZD7648 (MedChem Express 2230820-11-6) as described in the figure legends.

siRNA and Plasmid Transfection of Mammalian Cells

Cells were transfected with high quality maxiprepped plasmid DNA (Sigma Genelute HP kit), custom synthesized siRNA duplexes (Sigma-Aldrich VC30002), or Mission® siRNA Universal Negative Control #1 (Sigma Aldrich SIC001) using the jetPRIME transfection system (VWR 89129-926). For plasmid transfection, cells were grown to 70% confluence and transfected overnight with total µg of DNA added as recommended by supplier for the culture vessel. For siRNA transfection, knockdowns were performed per manufacturer suggestions in HeLa cells. Cells were transfected for 24 h after which the media was replaced with fresh media. Cells were allowed to grow for an additional 48 h before any additional treatment and harvesting.

Whole Cell Lysate Preparation and Western Blotting

Once experimental manipulations were complete, media was aspirated and cells were washed 3X with ice cold 1X TBS on ice. Cells were gently scraped into 1 mL ice cold 1X TBS and transferred to 1.5 mL microcentrifuge tubes. Cells were pelleted at 3000xg for 5 min at 4 °C, and the supernatant was aspirated. Pellets were stored at -80 °C until lysis.

1x RIPA lysis buffer (Cell Signaling Technology 9806S) supplemented with 1x Roche cOmplete protease inhibitor cocktail (Roche 11697498001), 1x Roche PhosStop (Roche 04906837001) or 1x Halt Phosphatase Inhibitor Cocktail (Thermo Scientific 78440), and 1 mM PMSF was added to the frozen pellets which were then agitated for 30 min at 4 °C then centrifuged at 16,000 xg for

504 15 min at 4 °C. Cleared lysates were transferred to a new tube, and protein concentrations were
505 quantified using the Pierce BCA Assay Kit (Thermo Scientific 23227). 30-100 µg total protein was
506 denatured in 1x SDS sample buffer with 10mM dithiothreitol (DTT) for 8 min at 95 °C. Lysates
507 were loaded onto polyacrylamide gels (8, 10% or Bio-Rad Mini-PROTEAN TGX Precast Protein
508 Gels, 4-20%) (BioRad) and separated by SDS-PAGE. Proteins were transferred to methanol-
509 activated 0.2 µm pore PVDF membranes overnight at 4 °C in 1X CAPS, 10% methanol.
510 Membranes were blocked in either 5% bovine serum albumin (BSA) (VWR) for phopsho-specific
511 antibodies, or 5% non-fat dry milk (BioRad) in TBS-T (0.1% Tween-20 in TBS) for 1 h at RT.
512 Primary antibodies were diluted in 5% BSA, 0.02% NaN_3 in TBS-T. Membranes were incubated
513 with primary antibody solutions overnight at 4°C. Membranes were washed 3X in TBS-T for 10
514 min each wash, then incubated with 1:5000 secondary antibody in blocking buffer for 1 h at RT.
515 Membranes were washed 3X in TBS-T for 10 min each wash, then developed for 1 min in
516 Amersham ECL Western Blotting Detection Reagent (Cytiva RPN2209) or Immobilon Crescendo
517 (Millipore WBLUR0500) and imaged on a ChemiDoc Imaging System (BioRad).
518
519 Phosphatase Sensitivity
520 HEK293T cells were treated with 10 mM MMS for 5h or left untreated. Following treatment, the
521 cells were harvested and split into two 1.5 mL microcentrifuge tubes per condition. Cells were
522 lysed in home-made RIPA buffer (20 mM Tris HCl pH 7.5, 150 mM NaCl, 1 mM EDTA, 1% Triton
523 X-100, 1% sodium deoxycholate, 0.1% SDS) supplemented with 1 mM PMSF, 1x PhosStop
524 (Roche 04906837001). The lysis buffer was further supplemented with 1x Roche PhosStop
525 (Roche 04906837001) or 1x Halt Phosphatase Inhibitor Cocktail (Thermo Scientific 78440) for
526 the '+ phosphatase inhibitor' samples. Lysis, protein quantification, and Western blots were
527 performed as described above.
528
529 Nuclear and Cytoplasmic Extraction
530 Nuclear and cytoplasmic extraction was performed at 4 °C using the NE-PER Nuclear and
531 Cytoplasmic Reagents (Fisher Scientific PI78835, Thermo Scientific 78833) following the
532 manufacturer's protocol. Protein quantification and Western blotting was performed as described
533 above.
534
535 Protein Purification
536 Hsc70 and point mutants were purified as described previously[61]. In brief, plasmids containing
537 His-tag proteins were transformed into Rosetta(DE3) *E. coli*. Bacteria were grown in 2 L Terrific
538 Broth (TB) to OD_{600}=0.6. Bacterial cultures were cooled to 20 °C, and protein expression was
539 induced with 200µM IPTG at 20 °C overnight. The cells were harvested by centrifugation (7500
540 r.p.m. 10 min, JLA 8.1 rotor) and then resuspended in 20 mL His-Binding Buffer (50 mM Tris, 10
541 mM imidazole, 500 mM NaCl, pH 8) + 2 tablets EDTA-free Roche cOmplete Protease Inhibitor
542 per liter culture using a Dounce homogenizer. Cells were then lysed by sonication at Amp 35%
543 for 5 min, 30 sec on, 30 sec off, on ice at 4 °C. Lysate was separated by centrifugation (18000
544 r.p.m. 30 min, JA-20 Beckman rotor) and incubated with 10 mL/L pre-equilibrated Ni-NTA resin
545 (EMD Millipore 70666-5)/liter of culture at 4 °C for 1 h. Bound protein was first washed with 200
546 mL His-binding buffer, then 100 mL His-Washing buffer (50 mM Tris, 30 mM imidazole, 300 mM
547 NaCl, pH 8) , and then eluted with His-Elution buffer (50 mM Tris, 300 mM imidazole, 300 mM
548 NaCl, pH 8). This His-tag was then removed by the spiking in 5 mM β-mercaptoethanol and 600
549 µg TEV protease to the sample and dialyzing overnight into Buffer A (25 mM HEPES, 5 mM $MgCl_2$,
550 10 mM KCl, pH 7.5) in 10 KDa MWCO snakeskin dialysis tubing (Thermo Fisher 68100). The
551 protein was further purified by an ATP-agarose column using previously established protocols[61].
552 Purified DnaJA2 and tau were acquired from J.E.G.
553
554 ATPase Assays with Malachite Green

555 The ATPase activity of Hsc70 and Hsc70(T495E) was performed with malachite green (MG)
556 (Sigma Aldrich) as described previously[62]. Briefly, in a clear 96-well plate, Hsc70 or Hsc70(T495E)
557 were incubated with increasing concentrations of human DnaJA2 (DJA2) in 25 µL total volume.
558 Reactions were also performed with DnaJA2 in the absence of Hsc70 for background subtraction.
559 The assay buffer was 100 mM Tris at pH 7.4, 20 mM KCl, 6 mM $MgCl_2$, and 0.01% Triton. The
560 reaction was initiated by the addition of ATP at a final concentration of 1 mM and incubated at
561 37 °C for 1 h. After incubation, 80 µL of MG reagent was added, followed by 10 µL of saturated
562 sodium citrate to quench the reaction. Absorbance was measured at 620 nm on a SpectraMax
563 M5 plate reader (Molecular Devices). ATP hydrolysis rates were calculated by comparison to a
564 phosphate standard. Displayed curves are a combination of 6 replicates.
565
566 Fluorescence Polarization (FP) of ATP-FAM
567 Nucleotide of Hsc70 and Hsc70(T495E) was assessed with a fluorescence polarization (FP)
568 assay using labeled ATP. First, apo-Hsc70 was generated by subsequent 6-12h dialyses in the
569 following buffers: buffer 1 (25 mM HEPES, 100 mM NaCl, 5 mM EDTA (pH 7.5)), buffer 2 (25 mM
570 HEPES, 100 mM NaCl, 1 mM EDTA (pH 7.5)), buffer 3 (25 mM HEPES, 5 mM $MgCl_2$, 10 mM KCl
571 (pH 7.5)). Following this, 40 kDa MWCO Zeba Buffer Exchange columns (Thermo Fisher A57760)
572 were used to exchange the buffer to FP assay buffer 100 mM Tris, 20 mM KCl, 6 mM $MgCl_2$, pH
573 7.4) before protein quantification. The assay was performed in 384-well black round-bottom low-
574 volume plates (Corning 4511). 40 nM ATP-FAM (Jena Bioscience nu-805-5fm) was added to
575 each well for a final concentration of 20 nM in 20 µL. Hsc70 and Hsc70(T495E) were added for a
576 starting concentration of 20 µM in 20 µL, and then serially diluted with FP assay buffer (2-fold 13
577 times into the ATP-FAM. Plates were covered and incubated for 30 min at room temperature.
578 Fluorescence polarization was read on a SpectraMax M5 plate reader (excitation, 485 nm;
579 emission, 535 nm)
580
581 Partial Proteolysis
582 The partial proteolysis protocol to identify Hsp70 conformations was modified from previous
583 work[18]. Hsc70 and Hsc70(T495E) was buffer exchanged to proteolysis buffer (40 mM HEPES,
584 20 mM NaCl, 8 mM $MgCl_2$, 20 mM KCl, 0.3 mM EDTA, pH 8) using Zeba 40 kDa MWCO buffer
585 exchange columns and diluted to 3 µM in this buffer. ATP or ADP was added to 1 mM and
586 incubated for 30 min at room temperature. 1.5 µM trypsin (Sigma EC 3.4.21.4) was added for 2 h
587 at room temperature. The reaction was quenched by boiling in SDS loading buffer (125 mM Tris-
588 HCl pH 6.8, 5% SDS, 10% β-mercaptoethanol, 20% glycerol, 0.025% bromophenol blue), run on
589 a precast SDS-PAGE gel (Bio-Rad) and stained by Coomassie.
590
591 Hsc70-tau binding ELISA
592 Hsc70-tau ELISA was modified from a previously published protocol[63]. It was performed in a
593 Fisherbrand, Flat bottom 96-well plates, clear, PS (cat no 12565501). 1µM Hsc70 or
594 Hsc70(T495E) (diluted in dialysis buffer 3 from FP assay) was added to wells along with 1 mM
595 ATP and incubated overnight at 37°C. Protein was discarded from wells followed by 3x 3min
596 washes on rocker with PBS-T, discarding the PBS-T and vigorously blotting the inverted plate on
597 a paper towel between each wash. In triplicate, add 30 uL of tau to each well, spanning a 12-dose
598 3-fold concentration gradient (from 70 µM). Plates were covered and incubated at room
599 temperature for 3 h. Solutions were removed and wells washed 3x with PBS-T as described above.
600 100 µL of blocking solution (5% non-fat milk in TBS-T) was added to all wells and incubated at
601 room temperature for 5 min without rocking. Solution was removed without washing. 50 uL of
602 primary antibody was added to all wells (1:2000 mouse anti-tau clone D-8 from SantaCruz
603 Biotechnologies in blocking solution). The plate was incubated for 1 h at room temperature without
604 shaking. Solution was removed and wells washed 3x with PBS-T. 50 µL of secondary antibody

605 (1:2000 goat anti-mouse (Jackson 115-035-146)in blocking solution) was added to the wells. The
606 plate was incubated for 1h at room temperature and then washed 3x with PBS-T. 50 µL of TMB
607 substrate was added to the wells (ThermoFisher 34028) and incubated for 15 min at room
608 temperature in the dark. 50 µL 1M HCl was added and the plate read at 450 nm on SpectraMax
609 M5 plate reader.
610
611 Yeast Strain Generation
612 W303α yeast and W303α yeast with SSA1 NAT were gifted to us by David Morgan. Oligos for
613 yeast point mutations were generated by PCR amplification of NAT-SSA1with the relevant codon
614 substituted in the primer sequence. Oligos for SSA2 interruption were generated by PCR
615 amplification of KanMX from pYM13 with flanking sequences to SSA2. gDNA was extracted from
616 yeast by first suspending yeast colonies from a YPAD plate in 100 µL LiOAc/SDS buffer (0.2 M
617 LiOAc, 1% SDS). Cells were incubated at 70 °C for 10 min, and then 300 µL 96-100% ethanol
618 was added. Sample was then mixed by vortexing. Sample was the spun at 15,000 xg for 3 min,
619 supernatant removed, and pellet dissolved in 100 µL nuclease free water. The sample was then
620 spun down at maximum speed for >15 sec, and supernatant was transferred to a new tube. 1 µL
621 of supernatant was used for subsequent PCRs.
622 For yeast transformations, competent cells were generated by first diluting an overnight culture
623 1:20 in YPAD and grown on a rotary shaker at 30 °C to mid-log. The yeast were spun at 3000 xg
624 for 1min. While spinning the yeast, 10 mg/mL salmon sperm DNA (Sigma-Aldrich D9156) was
625 boiled for 5 min and then put on ice. The supernatant was removed from the yeast pellet which
626 was then washed 1x in water and re-pelleted. The water was remove and the yeast was
627 resuspended in LiOAc/TE solution (10 mM Tris-HCl pH 8, 1 mM EDTA, 0.1 M lithium acetate
628 (Sigma-Aldrich L4158)). This was then pelleted, the supernatant aspirated, and yeast were
629 resuspended in 200 uL LiOAc/TE solution to generate competent cells. For each transformation,
630 50uL of these competent cells were mixed with 1µg of DNA along with 10 µL of boiled salmon
631 sperm DNA and 500 µL of PEG/LiOAc/TE solution (10 mM Tris-HCl pH 8, 1 mM EDTA, 0.1 M
632 lithium acetate, 40% PEG 3350). This mix was incubated at 30 °C with shaking at 550 r,p,m, on
633 a ThermoMixer F1.5 (Eppendorf), then spun for 1 min at 3000 xg. The supernatant was removed
634 and the yeast resuspended in sterile water and plated on YPAD and grown overnight at 30 °C.
635 The following day, these plates were replica plated onto plates with the appropriate selection
636 marker.
637
638 Yeast Growth
639 For all yeast experiments, yeast were first grown overnight in YPAD on a rotary shaker at 30 °C.
640 The following morning, yeast were diluted to OD_{600} =0.3 and grown at 30 °C to midlog (OD_{600} =
641 ~0.6). Strains were then concentrated (by centrifugation at 3000xg) to 2e7 cells/mL in 1.5 mL
642 microcentrifuge tubes.
643 Growth Curve
644 The above yeast were diluted 1:30 into a clear flat bottom 96 well plate (Costar 3370) and grown
645 for 25 h with continuous orbital shaking at 30 °C on a Cytation 5 Imaging Reader (BioTek) with
646 OD_{600} collected every 20 min.
647 Yeast Spot Test
648 The day prior to the experiment, Nunc Rectangular Dishes (Thermo 267060) were made with
649 either YPAD or YPAD + 0.0095% MMS. The above yeast were serially diluted 10-fold 5 times. 5
650 µL of the dilutions were spotted on the YPAD or YPAD + MMS plates. Plates were grown for three
651 days at 30 °C and imaged daily on a ChemiDoc Imaging System (BioRad).
652 Yeast Cell Cycle Analysis
653 This protocol was modified from previous work[64,65] For cell cycle analysis of yeast at mid-log, we
654 took 500 µL of the 2e7 cell/mL yeast solution, spun it at 14,000 xg for 30 sec, removed the

655 supernatant, washed 1x in water and re-pelleted. The water was then decanted, and the yeast
656 were vortexed to resuspend them in the water remaining in the tube. 95% ethanol prechilled to -
657 20 °C was added to the resuspended yeast which were then vortexed and placed on ice. For
658 MMS treatment, yeast were grown to mid-log as previously described. 0.05% MMS (Fisher
659 Scientific AC156890050) was then added to the yeast for 3 h[14], rotating at 30 °C. Samples were
660 harvested as described for 'no recovery' conditions, and the remaining yeast was transferred to
661 15 mL centrifuge tubes (Fisher Scientific 12-565-268),spun at 300 xg. The pellet was washed 1x
662 with sterile water, spun down again, and then resuspended in the starting volume of YPAD. The
663 caps were partially unscrewed and the yeast was returned to the rotary at 30 °C with samples
664 harvested as detailed above at the indicated time points. Once all samples were resuspended in
665 ethanol the yeast were stored at -20 °C for at least overnight. The yeast were then resuspended
666 by vortexing and spun at 14000 xg for 1 min. The ethanol was removed, the yeast resuspended
667 in water and then pelleted again. The water was removed and the pellet was resuspended in 1mL
668 sodium citrate buffer (50 mM sodium citrate (C8532), pH to 7.5 with citric acid (BP399)). 8 µL of
669 10 mg/mL RNAase A (Thermo EN0531) was then added to the samples and incubated for 2 h at
670 37 °C. Following this, 10 µL of 20 mg/mL Proteinase K (NEB P8107S) was added to the samples
671 and incubated for 1 h at 50 °C. The samples were then incubated at 4 °C overnight. The samples
672 were spun down at 14000 xg for 1 min and the pellets resuspended in 500 µL sodium citrate
673 buffer + 2.5 µM SYTOX Green (Thermo Fisher S7020), or sodium citrate buffer alone for the no-
674 stain control. Samples were placed on ice and sonicated with a probe sonicator (QSonica) at 30%
675 amplitude for 10 sec. The samples were then stored in the dark at 4 °C until flow cytometry
676 analysis.
677 All yeast flow cytometry experiments were performed on a LSRII SORP (BD Biosciences) using
678 a 488 nm laser, and the software analysis done on FlowJo (10.10.0). Cells were first selected by
679 graphing FSC-A by SSC-A. Singlets were then gated by graphing FSC-A by FSC-H and then
680 analyzed.
681 Yeast Lysis for Western Blotting
682 Yeast samples were treated as described, then 1 mL of sample was pelleted in a 1.5 mL
683 microcentrifuge tube at 13,000 xg for 1 min, washed 1x in water, pelleted at 13,000 xg, and then
684 the pellets were stored at -80 °C. The following day, the pellets were resuspended in 200 µL of
685 20% trichloroacetic acid (TCA). The samples were then centrifuged at 13,000 rpm for 30 sec at
686 4 °C. The supernatant was removed, and the pellets were washed with acetone prechilled in a -
687 20 °C freezer. The samples were spun at 13,000 rmp for 30 sec, the supernatant removed, and
688 the samples allowed to airdry at RT for ~10 min or until fully dry. The pellets were then
689 resuspended in 40 µL of 1M Tris pH 7.5, and then 200 µL of 2x Lamelli Buffer + 2% DTT was
690 added to each sample. Using a 200 µL PCR tube (VWR 53509-304), ~400 µL of 0.5 mm glass
691 disrupter beads (USA Scientific 7400-2405) were scooped into the sample and the sample was
692 beaten vigorously for 90 sec. With a 25 gauge needle, carefully hole was poked in the bottom of
693 the tube. The tube was then placed in a plastic vial (Falcon 352063), and spun with tops closed
694 at 500 xg for 3 min. The flowthrough was transferred to clean 1.5 mL microcentrifuge tube and
695 boiled for 10 min. Equal volumes of sample were then run in a 8-16% precast Mini-PROTEAN
696 TGX Stain Free gel (Bio-Rad 456-8103) per the manufacturer protocol. The Western block was
697 performed as described above.
698
699 Data Reproducibility and Statistical Analysis
700 All statistics were performed in Prism as described in the relevant figure legends. Figures are
701 either mean + SD, or representative of the number of replicates described in the figure legend.
702
703 **ACKNOWLEDGEMENTS**
704 We thank Dr. David Booth, Dr. Adriana Steinbach, and Dr. Michael Metrick for critical evaluation
705 and discussions of the data. We thank Dr. Henry Ng and Dr. David O. Morgan for yeast strains

and technical advice. We thank Dr. Oleta Johnson, Dr. Cory Nadel, and Dr. Emma Carroll from the J.E.G. lab for technical assistance and advice. We acknowledge Vinh Nguyen for his technical support and the PFCC (RRID:*SCR_018206*) for assistance generating Flow Cytometry data. Research reported here was supported in part by the DRC Center Grant NIH P30 DK063720. T.M. acknowledges support from the MPHD T32 training grant. J.E.G. acknowledges support from R01NS059690. S.M. acknowledges financial support from the National Institutes of Health (grant nos. R01GM140440 and R01GM144378), the Pew Charitable Trust (grant no. A129837), a Bowes Biomedical Investigator award, and is a Biohub, San Francisco, Investigator.

Author contributions

Conceptualization, T.M., S.M.; Experiment design, T.M., J.E.G., S.M.; Experimentation, T.M., A.W. K.B. M.C..; Formal Analysis, T.M..; Writing, T.M., S.M.; Review & Editing T.M, A.W., J.E.G., S.M.; Funding Acquisition: J.E.G., S.M.

REFERENCES

1. Rosenzweig, R., Nillegoda, N. B., Mayer, M. P. & Bukau, B. The Hsp70 chaperone network. *Nat. Rev. Mol. Cell Biol.* **20**, 665–680 (2019).

2. Kaushik, S. & Cuervo, A. M. The coming of age of chaperone-mediated autophagy. *Nat. Rev. Mol. Cell Biol.* **19**, 365–381 (2018).

3. Dubrez, L., Causse, S., Bonan, N. B., Dumétier, B. & Garrido, C. Heat-shock proteins: chaperoning DNA repair. *Oncogene* **39**, 516–529 (2020).

4. Truman, A. W. *et al.* CDK-Dependent Hsp70 Phosphorylation Controls G1 Cyclin Abundance and Cell-Cycle Progression. *Cell* **151**, 1308–1318 (2012).

5. Chen, Y.-J. *et al.* HSP70 colocalizes with PLK1 at the centrosome and disturbs spindle dynamics in cells arrested in mitosis by arsenic trioxide. *Arch. Toxicol.* **88**, 1711–1723 (2014).

6. Vergés, E., Colomina, N., Garí, E., Gallego, C. & Aldea, M. Cyclin Cln3 Is Retained at the ER and Released by the J Chaperone Ydj1 in Late G1 to Trigger Cell Cycle Entry. *Mol. Cell* **26**, 649–662 (2007).

7. Evans, C. G., Wisén, S. & Gestwicki, J. E. Heat Shock Proteins 70 and 90 Inhibit Early Stages of Amyloid β-(1–42) Aggregation in Vitro *. *J. Biol. Chem.* **281**, 33182–33191 (2006).

8. Valle-Medina, A., Calzada-Mendoza, C. C., Ocharan-Hernández, M. E., Jiménez-Zamarripa, C. A. & Juárez-Cedillo, T. Heat shock protein 70 in Alzheimer's disease and other dementias: A possible alternative therapeutic. *J. Alzheimer's Dis. Rep.* **9**, 25424823241307021 (2025).

9. Calderwood, S. K. & Murshid, A. Molecular Chaperone Accumulation in Cancer and Decrease in Alzheimer's Disease: The Potential Roles of HSF1. *Front. Neurosci.* **11**, 192 (2017).

10. Beltrao, P. *et al.* Systematic Functional Prioritization of Protein Posttranslational Modifications. *Cell* **150**, 413–425 (2012).

11. Preissler, S. *et al.* AMPylation matches BiP activity to client protein load in the endoplasmic reticulum. *eLife* **4**, e12621 (2015).

12. Preissler, S. *et al.* AMPylation targets the rate-limiting step of BiP's ATPase cycle for its functional inactivation. *eLife* **6**, e29428 (2017).

13. Moss, S. M. *et al.* A Legionella pneumophila Kinase Phosphorylates the Hsp70 Chaperone Family to Inhibit Eukaryotic Protein Synthesis. *Cell Host Microbe* **25**, 454-462.e6 (2019).

14. Albuquerque, C. P. *et al.* A Multidimensional Chromatography Technology for In-depth Phosphoproteome Analysis. *Mol. Cell. Proteom.* **7**, 1389–1396 (2008).

15. Holt, L. J. *et al.* Global Analysis of Cdk1 Substrate Phosphorylation Sites Provides Insights into Evolution. *Science* **325**, 1682–1686 (2009).

16. Russell, R., Karzai, A. W., Mehl, A. F. & McMacken, R. DnaJ Dramatically Stimulates ATP Hydrolysis by DnaK: Insight into Targeting of Hsp70 Proteins to Polypeptide Substrates †. *Biochemistry* **38**, 4165–4176 (1999).

757 17. Preissler, S., Rato, C., Perera, L. A., Saudek, V. & Ron, D. FICD acts bifunctionally to
758 AMPylate and de-AMPylate the endoplasmic reticulum chaperone BiP. *Nat. Struct. Mol. Biol.* **24**,
759 23–29 (2017).
760 18. Rinaldi, S. *et al.* A Local Allosteric Network in Heat Shock Protein 70 (Hsp70) Links Inhibitor
761 Binding to Enzyme Activity and Distal Protein–Protein Interactions. *ACS Chem. Biol.* **13**, 3142–
762 3152 (2018).
763 19. Buchberger, A. *et al.* Nucleotide-induced Conformational Changes in the ATPase and
764 Substrate Binding Domains of the DnaK Chaperone Provide Evidence for Interdomain
765 Communication (*). *J. Biol. Chem.* **270**, 16903–16910 (1995).
766 20. Kundel, F. *et al.* Hsp70 Inhibits the Nucleation and Elongation of Tau and Sequesters Tau
767 Aggregates with High Affinity. *ACS Chem. Biol.* **13**, 636–646 (2018).
768 21. Lee, P.-C. & Machner, M. P. The Legionella Effector Kinase LegK7 Hijacks the Host Hippo
769 Pathway to Promote Infection. *Cell Host Microbe* **24**, 429-438.e6 (2018).
770 22. Thomas, E. N., Kim, K. Q., McHugh, E. P., Marcinkiewicz, T. & Zaher, H. S. Alkylative damage
771 of mRNA leads to ribosome stalling and rescue by trans translation in bacteria. *eLife* **9**, e61984
772 (2020).
773 23. Beard, W. A., Horton, J. K., Prasad, R. & Wilson, S. H. Eukaryotic Base Excision Repair: New
774 Approaches Shine Light on Mechanism. *Annu. Rev. Biochem.* **88**, 137–162 (2019).
775 24. Sedgwick, B. Repairing DNA-methylation damage. *Nat. Rev. Mol. Cell Biol.* **5**, 148–157 (2004).
776 25. Wyatt, M. D. & Pittman, D. L. Methylating Agents and DNA Repair Responses: Methylated
777 Bases and Sources of Strand Breaks. *Chem. Res. Toxicol.* **19**, 1580–1594 (2006).
778 26. Fu, D., Calvo, J. A. & Samson, L. D. Balancing repair and tolerance of DNA damage caused
779 by alkylating agents. *Nat. Rev. Cancer* **12**, 104–120 (2012).
780 27. Sobol, R. W. *et al.* Base Excision Repair Intermediates Induce p53-independent Cytotoxic
781 and Genotoxic Responses*. *J. Biol. Chem.* **278**, 39951–39959 (2003).
782 28. Srivastava, D. K. *et al.* Mammalian Abasic Site Base Excision Repair IDENTIFICATION OF
783 THE REACTION SEQUENCE AND RATE-DETERMINING STEPS*. *J. Biol. Chem.* **273**, 21203–
784 21209 (1998).
785 29. Horton, J. K., Prasad, R., Hou, E. & Wilson, S. H. Protection against Methylation-induced
786 Cytotoxicity by DNA Polymerase β-Dependent Long Patch Base Excision Repair*. *J. Biol. Chem.*
787 **275**, 2211–2218 (2000).
788 30. Bau, D.-T. *et al.* Oxidative DNA adducts and DNA-protein cross-links are the major DNA
789 lesions induced by arsenite. *Environ. Heal. Perspect.* **110**, 753–756 (2002).
790 31. Ebert, F. *et al.* Arsenicals affect base excision repair by several mechanisms. *Mutat.*
791 *Res.Fundam. Mol. Mech. Mutagen.* **715**, 32–41 (2011).
792 32. Sykora, P. & Snow, E. T. Modulation of DNA polymerase beta-dependent base excision repair
793 in cultured human cells after low dose exposure to arsenite. *Toxicol. Appl. Pharmacol.* **228**, 385–
794 394 (2008).
795 33. Caldecott, K. W. Single-strand break repair and genetic disease. *Nat. Rev. Genet.* **9**, 619–
796 631 (2008).
797 34. Nikolova, T., Ensminger, M., Löbrich, M. & Kaina, B. Homologous recombination protects
798 mammalian cells from replication-associated DNA double-strand breaks arising in response to
799 methyl methanesulfonate. *DNA Repair* **9**, 1050–1063 (2010).
800 35. Ensminger, M. *et al.* DNA breaks and chromosomal aberrations arise when replication meets
801 base excision repair. *J. Cell Biol.* **206**, 29–43 (2014).
802 36. Polyzos, A. A. *et al.* Base excision repair and double strand break repair cooperate to
803 modulate the formation of unrepaired double strand breaks in mouse brain. *Nat. Commun.* **15**,
804 7726 (2024).
805 37. Giglia-Mari, G., Zotter, A. & Vermeulen, W. DNA Damage Response. *Cold Spring Harb.*
806 *Perspect. Biol.* **3**, a000745 (2011).

807 38. Durocher, D. & Jackson, S. P. DNA-PK, ATM and ATR as sensors of DNA damage: variations
808 on a theme? *Curr. Opin. Cell Biol.* **13**, 225–231 (2001).
809 39. Lowndes, N. F. & Murguia, J. R. Sensing and responding to DNA damage. *Curr. Opin. Genet.*
810 *Dev.* **10**, 17–25 (2000).
811 40. Caron, P. *et al.* Non-redundant Functions of ATM and DNA-PKcs in Response to DNA Double-
812 Strand Breaks. *Cell Rep.* **13**, 1598–1609 (2015).
813 41. Heijink, A. M., Krajewska, M. & Vugt, M. A. T. M. van. The DNA damage response during
814 mitosis. *Mutat. Res.Fundam. Mol. Mech. Mutagen.* **750**, 45–55 (2013).
815 42. Lanz, M. C., Dibitetto, D. & Smolka, M. B. DNA damage kinase signaling: checkpoint and
816 repair at 30 years. *EMBO J.* **38**, EMBJ2019101801 (2019).
817 43. Choi, S., Gamper, A. M., White, J. S. & Bakkenist, C. J. Inhibition of ATM kinase activity does
818 not phenocopy ATM protein disruption. *Cell Cycle* **9**, 4052–4057 (2010).
819 44. Menolfi, D. & Zha, S. ATM, ATR and DNA-PKcs kinases—the lessons from the mouse models:
820 inhibition ≠ deletion. *Cell Biosci.* **10**, 8 (2020).
821 45. Zannini, L., Delia, D. & Buscemi, G. CHK2 kinase in the DNA damage response and beyond.
822 *J. Mol. Cell Biol.* **6**, 442–457 (2014).
823 46. Tuppi, M. *et al.* Oocyte DNA damage quality control requires consecutive interplay of CHK2
824 and CK1 to activate p63. *Nat. Struct. Mol. Biol.* **25**, 261–269 (2018).
825 47. Canman, C. E. *et al.* Activation of the ATM Kinase by Ionizing Radiation and Phosphorylation
826 of p53. *Science* **281**, 1677–1679 (1998).
827 48. Chou, W.-C., Hu, L.-Y., Hsiung, C.-N. & Shen, C.-Y. Initiation of the ATM-Chk2 DNA damage
828 response through the base excision repair pathway. *Carcinogenesis* **36**, 832–840 (2015).
829 49. Werner-Washburne, M., Stone, D. E. & Craig, E. A. Complex Interactions Among Members
830 of an Essential Subfamily of hsp70 Genes in Saccharomyces Cerevisiae. *Mol. Cell. Biol.* **7**, 2568–
831 2577 (1987).
832 50. Craig, E. A. & Jacobsen, K. Mutations of the heat inducible 70 kilodalton genes of yeast confer
833 temperature sensitive growth. *Cell* **38**, 841–849 (1984).
834 51. Moreno, D. F. *et al.* Proteostasis collapse, a hallmark of aging, hinders the chaperone-Start
835 network and arrests cells in G1. *eLife* **8**, e48240 (2019).
836 52. Caldecott, K. W. Mammalian DNA base excision repair: Dancing in the moonlight. *DNA Repair*
837 **93**, 102921 (2020).
838 53. Hantschel, O. Unexpected Off-Targets and Paradoxical Pathway Activation by Kinase
839 Inhibitors. *ACS Chem. Biol.* **10**, 234–245 (2015).
840 54. Jackson, A. L. & Linsley, P. S. Recognizing and avoiding siRNA off-target effects for target
841 identification and therapeutic application. *Nat. Rev. Drug Discov.* **9**, 57–67 (2010).
842 55. Blackford, A. N. & Stucki, M. How Cells Respond to DNA Breaks in Mitosis. *Trends Biochem.*
843 *Sci.* **45**, 321–331 (2020).
844 56. Pramanik, S., Chen, Y. & Bhakat, K. K. Base Excision Repair in Mitotic Cells and the Role of
845 Apurinic/Apyrimidinic Endonuclease 1 (APE1) in Post-Mitotic Transcriptional Reactivation of
846 Genes. *Int. J. Mol. Sci.* **25**, 12735 (2024).
847 57. Fontaine, S. N. *et al.* Isoform-selective Genetic Inhibition of Constitutive Cytosolic Hsp70
848 Activity Promotes Client Tau Degradation Using an Altered Co-chaperone Complement*. *J. Biol.*
849 *Chem.* **290**, 13115–13127 (2015).
850 58. Muller, P. *et al.* C-terminal phosphorylation of Hsp70 and Hsp90 regulates alternate binding
851 to co-chaperones CHIP and HOP to determine cellular protein folding/degradation balances.
852 *Oncogene* **32**, 3101–3110 (2013).
853 59. Nitika & Truman, A. W. Cracking the Chaperone Code: Cellular Roles for Hsp70
854 Phosphorylation. *Trends Biochem. Sci.* **42**, 932–935 (2017).
855 60. Pettersen, E. F. *et al.* UCSF Chimera—A visualization system for exploratory research and
856 analysis. *J. Comput. Chem.* **25**, 1605–1612 (2004).

857 61. Chang, L., Thompson, A. D., Ung, P., Carlson, H. A. & Gestwicki, J. E. Mutagenesis Reveals
858 the Complex Relationships between ATPase Rate and the Chaperone Activities of Escherichia
859 coli Heat Shock Protein 70 (Hsp70/DnaK)*. *J. Biol. Chem.* **285**, 21282–21291 (2010).
860 62. Chang, L. *et al.* High-throughput screen for small molecules that modulate the ATPase activity
861 of the molecular chaperone DnaK. *Anal. Biochem.* **372**, 167–176 (2008).
862 63. Nadel, C. M. *et al.* Phosphorylation of tau at a single residue inhibits binding to the E3 ubiquitin
863 ligase, CHIP. *Nat. Commun.* **15**, 7972 (2024).
864 64. Zhang, H. & Siede, W. Cell Cycle Checkpoint Control Protocols. *Methods Mol. Biol. (Clifton,*
865 *NJ)* **241**, 77–91 (2003).
866 65. Rosebrock, A. P. Analysis of the Budding Yeast Cell Cycle by Flow Cytometry. *Cold Spring*
867 *Harb. Protoc.* **2017**, pdb.prot088740 (2017).
868 66. Omkar, S. *et al.* Mechanosensor-mediated Hsp70 phosphorylation orchestrates the
869 landscape of the heat shock response. *Nat. Commun.* **17**, 507 (2025).
870 67. Backe, S. J., Heritz, J. A. & Mollapour, M. Hsp70 and Hsp90 post-translational modifications
871 and translating the chaperone code. *Cell Stress Chaperones* **30**, 100118 (2025).

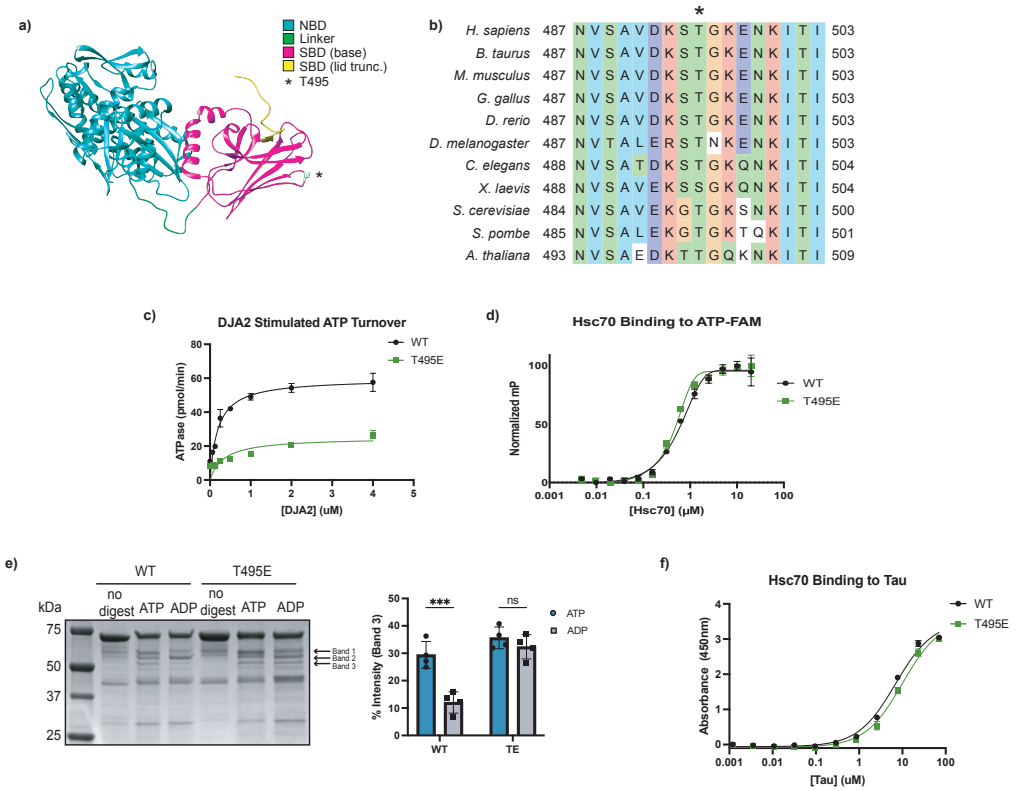

Figure 1. The phosphomimetic Hsc70 T495E mutant adopts an open-like conformation
a) Crystal structure of bovine Hsc70(residues 1-554; PDB: 1YUW). The nucleotide-binding domain (NBD, residues 1-383) is shown in cyan, the interdomain linker (residues 384-394) in green, and the substrate binding domain (SBD, residues 395-506) in magenta. T495 is highlighted in white and marked with an asterisk. **b)** Multiple sequence alignment of cytosolic Hsp70 orthologs. Human (P11142), mouse (P63017), cow (P19120), chicken (O73885), zebrafish (Q90473, fruit fly (P11147), worm (P09446), budding yeast (P10591), fission yeast (Q10265), and *Arabidopsis* (P22953) Hsc70 UniProt sequences were aligned with MAFFT (v7). Coloring follows CLUSTAL conventions; T495 is marked with an asterisk (*). **c)** J-protein-stimulated ATPase activity of wild-type (WT) and phosphomimetic Hsc70 (T495E) measured by malachite green assay. Data points represent mean + SD of technical triplicates. **d)** Fluorescence polarization of ATP-FAM binding to WT and T495E Hsc70. Values were normalized to the minimum and maximum polarization; data points represent mean + SD of technical triplicates. **e)** Partial proteolysis of WT and T495E Hsc70 by trypsin in the presence of ATP or ADP. Digestion products were resolved by SDS-PAGE and visualized with a Coomassie stain, and band intensities were quantified (bar graph, right). Statistical significance was determined by two-way ANOVA with Šidák's multiple comparisons test (adjusted p = 0.0002, n = 4 technical replicates). **f)** Tau binding to immobilized WT and T495E Hsc70 measured by ELISA. Data points represent mean + SD of technical triplicates.

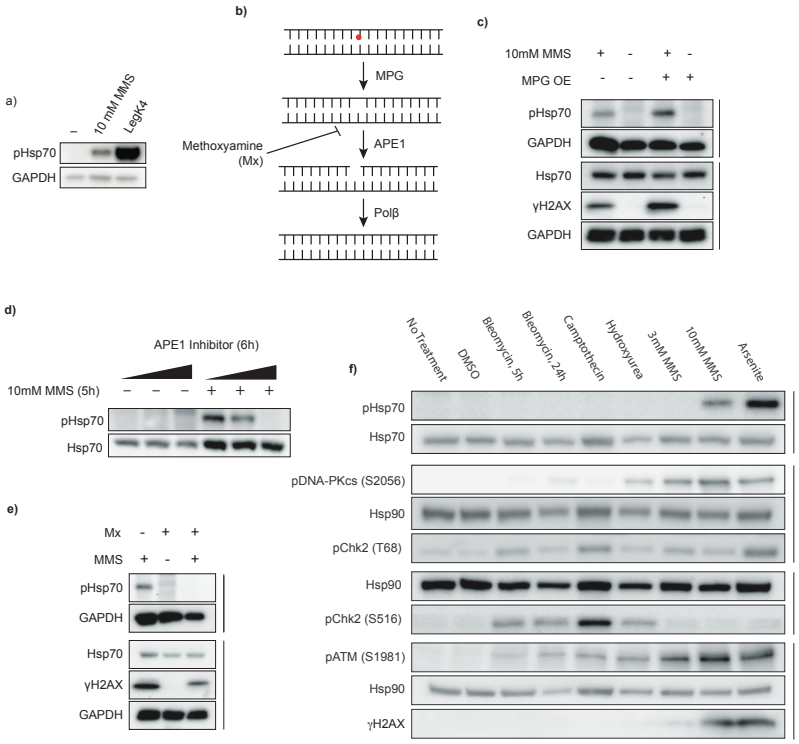

Figure 2. Base excision repair drives phosphorylation of Hsp70 in human cells
a) Hsp70 phosphorylation by MMS treatment or LegK4 overexpression. HEK293T cells were transiently transfected overnight with LegK4Δ1-58:GFP or treated with 10 mM MMS for 5 h. Phosphorylation at T495 was detected using a phospho-specific antibody to pHsp70 T495; GAPDH was used as a loading control. Data are representative of n > 3 independent experiments. **b)** Schematic of the base excision repair (BER) pathway, highlighting steps relevant to MMS-induced DNA damage. **c)** MPG overexpression increases pHsp70 levels. HEK293T cells were transiently transfected with MPG overnight, treated with MMS, and analyzed by immunoblotting for pHsp70, the loading controls GAPDH and Hsp70, and the DNA damage marker γH2AX. Data are representative of n = 3 independent experiments. **d)** Inhibition of APE1 reduces MMS-induced pHsc70. Cells were pretreated for 1h with 5μM, 10 μM, or 50 μM APE1 inhibitor (APE1 compound III) before MMS treatment. Hsp70 and pHsp70 were detected by immunoblotting. Data are representative of n = 3 independent experiments. **e)** Masking of AP sites prevents pHsp70 accumulation. Cells were pretreated with 60 mM methoxyamine (Mx) for 30 min, followed by cotreatment with 30 mM Mx and 10 mM MMS for 5 h. pHsp70, the loading controls GAPDH and Hsp70, and the DNA damage marker γH2AX were detected by immunoblotting. Data are representative of n = 3 independent experiments. **f)** DNA damage specificity panel for pHsp70 induction. Cells were treated with bleomycin (10 μM, 5 h or 24 h), camptothecin (10 μM, 5 h), hydroxyurea (2 mM, 24 h), MMS (3 mM or 10 mM, 5 h), sodium arsenite (0.5 mM, 5 h), or DMSO vehicle (5 h). Immunoblotting was performed for pHsp70, DDR kinase activation markers (pDNA-PKcs S2056, pChk2 T68, pChk2 S16, pATM S1981), DNA damage marker γH2AX, and loading controls (Hsp70 and Hsp90). Data are representative of n = 3 independent experiments.

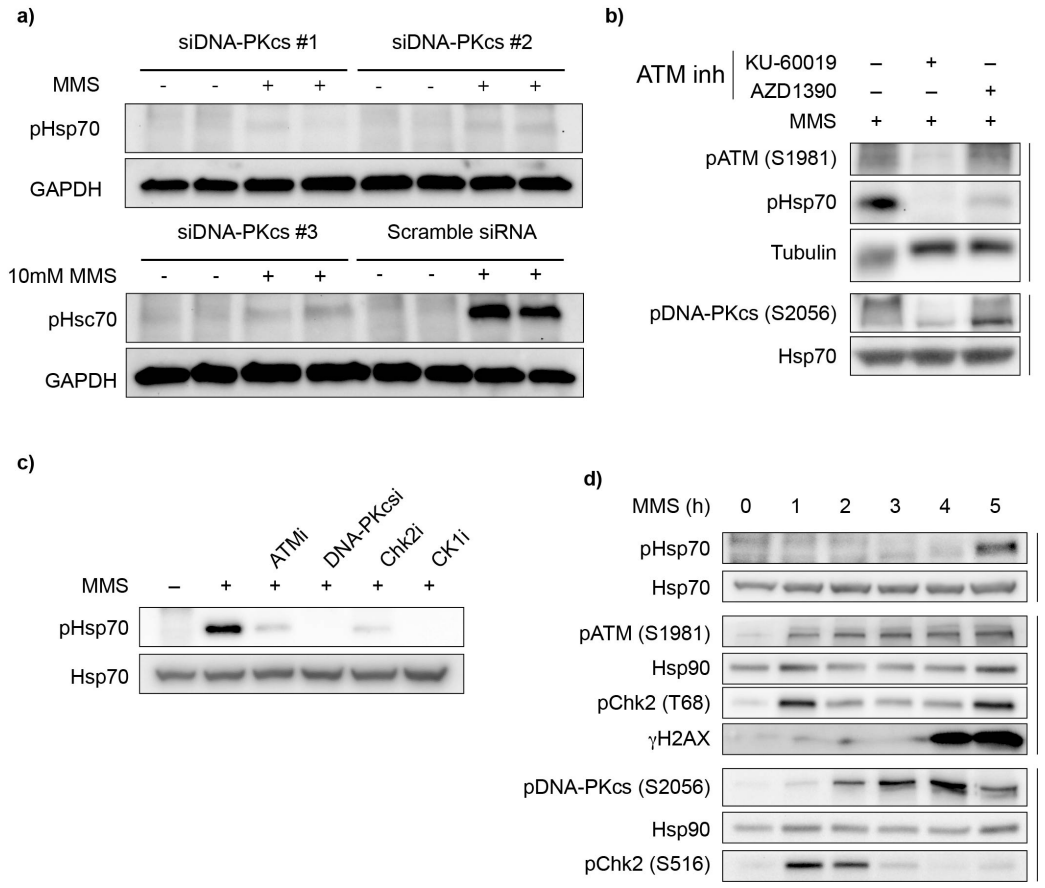

Figure 3. DDR kinase activity is upstream of Hsp70 phosphorylation
a) DNA-PKcs knockdown reduces pHsp70 levels. Cells were transiently transfected with three independent siRNAs targeting DNA-PKcs or a scramble control for 72 h, followed by treatment with 10 mM MMS for 5 h. pHsp70 and GAPDH (loading control) were detected by immunoblotting. Data are representative of n = 3 independent experiments. **b)** Pharmacological inhibition of ATM decreases pHsp70 induction. Cells were pretreated for 1 h with ATM inhibitors (10 μM KU-60019 or 200nM AZD1390), then treated with 10 mM MMS for 5 h. ATM and DNA-PKcs autoactivation were monitored by immunoblotting pATM (S1981) and pDNA-PKcs (S2056), respectively. Tubulin and total Hsp70 served as loading controls. Data are representative of n = 3 independent experiments. **c)** Pharmacological inhibition of ATM, DNA-PKcs, Chk2, and CK1 decrease Hsp70 phosphorylation during MMS treatment. Cells were pretreated for 1h with inhibitors for ATM (200 nM AZD1390), DNA-PKcs (2 μM AZD7648), Chk2 (5 μM CCT241533), CK1(50 μM PF-670462) or with vehicle control (DMSO), then treated with 10mM MMS for 5h. Immunoblotting was performed against pHsp70 and the loading control Hsp70. Data are representative of n = 3 independent experiments. **d)** Timecourse of MMS-induced DDR activation and pHsp70 phosphorylation. Cells were treated with 10 mM MMS and harvested hourly. ATM and DNA-PKcs activation were detected by pATM (S1981) and pDNA-PKcs (S2056), respectively. Chk2 activation was monitored by pChk2 (T68) and pChk2 (S516). DNA damage was assessed via γH2AX. Hsp70 and Hsp90 were used as loading controls. Data are representative of n = 3 independent experiments

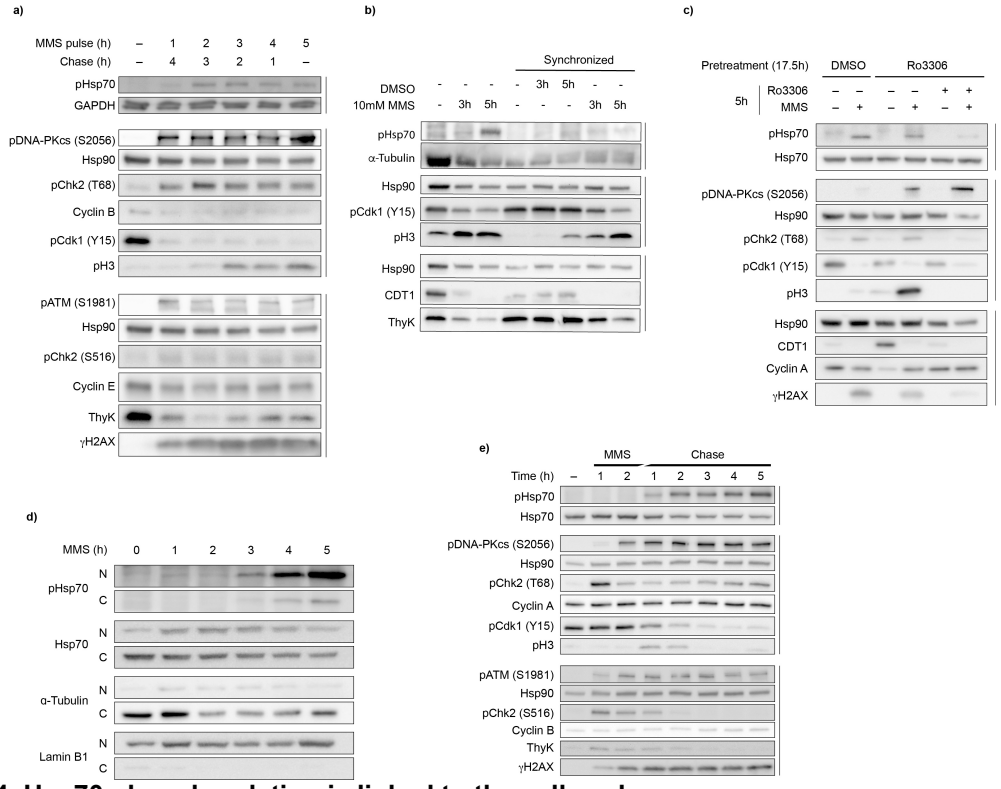

Figure 4. Hsp70 phosphorylation is linked to the cell cycle

a) Variable pulse-chase MMS treatment suggests a complex signaling pathway. Cells were treated with 10 mM MMS for 1-5 h, washed, then incubated in MMS-free media for the remainder of the 5 h period. ATM and DNA-PKcs activation were detected by pATM (S1981) and pDNA-PKcs (S2056); Chk2 activation by pChk2 (T68) and pChk2 (S516); DNA damage by γH2AX. Cell cycle progression was monitored with S phase markers thymidine kinase (ThyK) and CDT1; mitotic entry marker pCdk1(Y15) (dephosphorylation permits M-phase entry), M phase marker phospho-histone H3 (S10) (pH3); and cyclins B and E. GAPDH and Hsp90 are loading controls. Data are representative of n = 3 independent experiments. **b)** Early S-phase synchronization fails to increase pHsp70 accumulation. Cells were synchronized with 2.5 mM thymidine (18 h → 9 h release → 17 h retreatment), and released into fresh media ±10 mM MMS for the indicated times. Asynchronous cells were also MMS treated. Immunoblots were performed for pHsp70, cell cycle markers (pCdk1 Y15, pH3, CDT1, ThyK), and loading controls α-tubulin and Hsp90. Data are representative of n = 2 independent experiments. **c)** G2/M stalling by CDK1 inhibition reduces pHsp70 levels. Cells were pretreated with 10 μM CDK1 inhibitor Ro3306 or DMSO for 17.5 h, washed, then treated again with Ro3306 or DMSO ±10 mM MMS for 5 h. Immunoblotting was performed for pHsp70, cell cycle markers(pCdk1 Y15, pH3, CDT1, cyclin A), DDR markers (pDNA-PKcs S2056, pChk2 T68, γH2AX), and loading controls Hsp70 and Hsp90. Data are representative of n = 3 independent experiments. **d)** Subcellular fractionation of pHsp70 during MMS treatment shows nuclear localization. Cells were treated with 10 mM MMS from 1-5 h or left untreated. Cytoplasmic and nuclear extracts were prepared using the NE-PER kit. Immunoblotting was performed for pHsp70 and total Hsp70 levels; α-tubulin and lamin B1 served as cytoplasmic and nuclear markers, respectively. Data are representative of n = 3 independent experiments. **e)** A 2 h MMS pulse chase reveals pHsp70 accumulation post-mitosis. Cells were treated with 10 mM MMS for 2 h, washed, and then incubated in fresh media. Samples were harvested hourly, alongside an untreated control. Immunoblotting was performed for pHsp70, DDR markers (pDNA-PKcs S2056, pChk2 T68, pATM S1981, pChk2 S516, γH2AX), cell cycle markers (cyclin A, pCdk1 Y15, pH3, cyclin B, ThyK), and loading controls Hsp70 and Hsp90. Data are representative of n = 3 independent experiments.

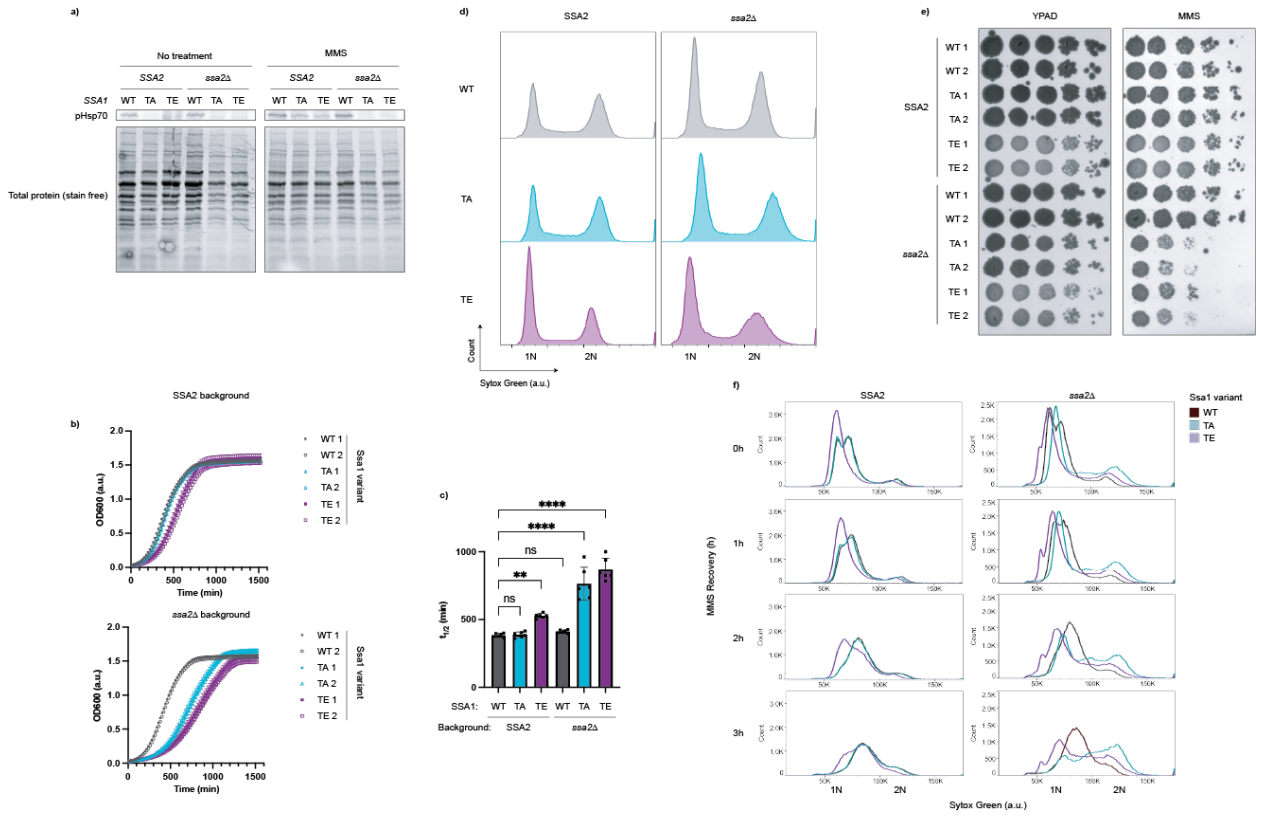

Figure 5. Ssa1 T492 phosphorylation mutations cause cell cycle defects in *S. cerevisiae*
a) Phosphorylation of Hsp70 is conserved in yeast. Strains were grown to mid-log and treated with 0.05% MMS in YPAD or fresh YPAD for 3 h. Immunoblots were performed for pHsp70 and total protein (StainFree, BioRad) was used as a loading control. Data are representative of n = 2 experiments. **b)** Growth curves of *S. cerevisiae* Ssa1 mutants show delayed growth. Indicated strains were grown to mid-log phase, diluted to the same starting concentration, and monitored overnight at 30 °C in a plate reader. Data represent the average of technical triplicates. Data are representative of n = 3 independent experiments. **c)** Half-times ($t_{1/2}$) of both Ssa1 mutants in the *ssa2*Δ background, and of the phosphomimetic mutant in the *SSA2* background, are significantly increased. Sigmoidal fits were applied to growth curves to determine $t_{1/2}$ values. The data represent three technical replicates with two biological replicates per strain. Bars represent mean + SD of six replicates (n = 6; 2 biological replicates x 3 technical replicates) Statistical significance was determined by ordinary one-way ANOVA followed by Dunnett's multiple comparison test (** $p = 0.0015$; **** $p < 0.0001$). **d)** Cell cycle distribution analysis reveals G1 stalling of Ssa1 phosphomutants. Yeast were grown to mid-log phase, adjusted to the same concentration, and immediately fixed. Cells were stained with Sytox Green and analyzed by flow cytometry to determine DNA content. Histograms display DNA content (X-axis) with 1N corresponding to G1 phase, 2N to G2/M, and intermediate values to S phase. Left: WT *SSA2* background; right: *ssa2*Δ background. Data are representative of n = 4 technical replicates with 2 biological replicates per strain. **e)** Ssa1 phosphomutants display increased MMS sensitivity in a spot test assay. Yeast were grown to mid-log phase, adjusted to 2e7 cells/mL, serially diluted 1:10, and spotted (5µL) onto YPAD plates with or without 0.0095% MMS. Plates were incubated at 30 °C and imaged after 3 days. Data are representative of n = 3 independent experiments. **f)** Ssa1 phosphomutants exhibit perturbed G1/S stalling during MMS recovery. Yeast were grown to mid-log phase, treated with 0.05% MMS for 3 h, washed, and resuspended in fresh media for recovery. Samples were collected at the indicated times points and analyzed by staining and flow cytometry as described as in (d). Data are representative of n = 2 technical replicates with 2 biological replicates per strain.